Inorg. Chem. **2008**, *47*, 6203−6211

Quenching Mechanism of Zn(Salicylaldimine) by Nitroaromatics

Meaghan E. Germain,[†] Thomas R. Vargo,[†] Beth Anne McClure,[‡] Jeffrey J. Rack,[‡] P. Gregory Van Patten,[‡] Michael Odoi,[†] and Michael J. Knapp*[,†,§]

Department of Chemistry and Program in Molecular and Cellular Biology, University of Massachusetts at Amherst, Amherst, Massachusetts 01003, and Department of Chemistry and Biochemistry, Ohio University, Athens, Ohio 45701

Received December 20, 2007

Nitroaromatics and nitroalkanes quench the fluorescence of Zn(Salophen) (H_2Salophen = *N,N*′-phenylene-bis-(3,5-di-*tert*-butylsalicylideneimine); **ZnL^R**) complexes. A structurally related family of **ZnL^R** complexes (R = OMe, di-*t*Bu, *t*Bu, Cl, NO_2) were prepared, and the mechanisms of fluorescence quenching by nitroaromatics were studied by a combined kinetics and spectroscopic approach. The fluorescent quantum yields for **ZnL^R** were generally high ($\Phi \sim 0.3$) with sub-nanosecond fluorescence lifetimes. The fluorescence of **ZnL^R** was quenched by nitroaromatic compounds by a mixture of static and dynamic pathways, reflecting the **ZnL^R** ligand bulk and reduction potential. Steady-state Stern-Volmer plots were curved for **ZnL^R** with less-bulky substituents (R = OMe, NO_2), suggesting that both static and dynamic pathways were important for quenching. Transient Stern-Volmer data indicated that the dynamic pathway dominated quenching for **ZnL^R** with bulky substituents (R = *t*Bu, D*t*Bu). The quenching rate constants with varied nitroaromatics ($ArNO_2$) followed the driving force dependence predicted for bimolecular electron transfer: **ZnL*** + $ArNO_2$ → **ZnL**$^+$ + $ArNO_2^-$. A treatment of the diffusion-corrected quenching rates with Marcus theory yielded a modest reorganization energy (λ = 25 kcal/mol), and a small self-exchange reorganization energy for **ZnL***/**ZnL**$^+$ (ca. 20 kcal/mol) was estimated from the Marcus cross-relation, suggesting that metal phenoxyls may be robust biological redox cofactors. Electronic structure calculations indicated very small changes in bond distances for the **ZnL** → **ZnL**$^+$ oxidation, suggesting that solvation was the dominant contributor to the observed reorganization energy. These mechanistic insights provide information that will be helpful to further develop **ZnL^R** as sensors, as well as for potential photoinduced charge transfer chemistry.

Introduction

The detection of nitro-containing compounds is important for sensing explosives such as trinitrotoluene and dinitrotoluene (DNT), the primary components in millions of unexploded landmines, as well as chemical taggants legally required in plastic explosives, such as 2,3-dimethyl-2,3-dinitrobutane (DMNB).[1–5] Methods of detection include metal detectors, which are ineffective toward plastics, and trained canines, which are extremely expensive due to training and care. Most other methods such as X-ray dispersion, mass spectrometry, and nuclear quadrupole resonance require large, expensive instrumentation, introducing difficulties in the development of portable devices.[6] Transduction methods such as absorption, fluorescence, and conductivity have been used because of their high sensitivity, but selectivity for aromatic and aliphatic nitro compounds remains a challenge for sensor development.[1,7–9] Nevertheless, fluorescence detection combines the promise of high

* To whom correspondence should be addressed. E-mail: mknapp@chem.umass.edu.
† Department of Chemistry, University of Massachusetts at Amherst.
‡ Program in Molecular and Cellular Biology, University of Massachusetts at Amherst.
§ Ohio University.

(1) Yang, J. S.; Swager, T. M. *J. Am. Chem. Soc.* **1998**, *120* (46), 11864–11873.
(2) Maureen, R. A. *C&E News* **1997**, 14.
(3) Liu, Y.; Mills, R. C.; Boncella, J. M.; Schanze, K. S. *Langmuir* **2001**, *17* (24), 7452–7455.
(4) Czarnik, A. W. *Nature* **1998**, *394* (6692), 417–418.
(5) Moore, D. S. *Rev. Sci. Instrum.* **2004**, *75* (8), 2499–2512.
(6) Toal, S. J.; Trogler, W. C. *J. Mater. Chem.* **2006**, *16* (28), 2871–2883.
(7) Goodpaster, J. V.; McGuffin, V. L. *Anal. Chem.* **2001**, *73* (9), 2004–2011.
(8) Albert, K. J.; Walt, D. R. *Anal. Chem.* **2000**, *72* (9), 1947–1955.
(9) Albert, K. J.; Lewis, N. S.; Schauer, C. L.; Sotzing, G. A.; Stitzel, S. E.; Vaid, T. P.; Walt, D. R. *Chem. Rev.* **2000**, *100* (7), 2595–2626.

10.1021/ic702469q CCC: $40.75
Published on Web 06/25/2008

sensitivity with the ease of use that is needed for widely accessible explosives detection.

Polymeric sensors, such as poly(phenylene ethynylene)[10–12] and polymetalloles,[6,13] rely on electron-rich aromatic rings that can π-stack with the electron-poor nitroaromatics for effective binding. Although these polymers can be highly sensitive, important nitro-aliphatic analytes lack the aromatic rings necessary for tight binding. For example, DMNB is a common taggant for explosives detection, but it is incapable of π-stacking, making it difficult to detect by binding. DMNB also lacks a visible absorption band, and therefore it is unlikely to undergo energy-transfer-based quenching. Electron-transfer-based quenching would provide a mechanism to detect a broad range of explosives, including DMNB. While it has been reported that these polymeric sensors are quenched by electron transfer with the bound nitroaromatics,[10,13,14] supporting data for this mechanism is indirect.

Zn(salicylaldimine) complexes have been reported to possess excellent photophysical properties for fluorescence sensing, such as nanosecond lifetimes and high quantum yields, and also undergo efficient energy transfer.[15,16] We have recently reported a Zn(Salophen) (H_2Salophen = *N*,*N*′-phenylene-bis-(3,5-di-*tert*-butylsalicylideneimine); $\mathbf{ZnL^{DtBu}}$) complex, which exhibits steady-state fluorescence quenching with nitroaromatics and DMNB.[17a] To determine if this quenching mechanism is indeed a photoinduced electron transfer event and to describe the energy barriers associated with quenching, we synthesized a family of $\mathbf{ZnL^R}$ complexes that alter the reduction potential according to the electron-donating or -accepting properties of the 5-substituent on the phenolate ring (Scheme 1). Typical complexes were found to have high quantum yields ($\Phi \sim 0.3$) and to be quenched by nitro-organics. Electron transfer from $\mathbf{ZnL^R}$ to the nitroaromatic is demonstrated through the driving force dependence of quenching rates, as well as by the formation of an electron paramagnetic resonance (EPR)-active phenoxyl radical that is coordinated to Zn^{2+}, related to other 5-coordinate metal centers with appended phenoxyls.[18] Transient and steady-state Stern-Volmer quenching plots indicated that quenching occurred by a mixture of static and dynamic pathways which depend primarily on the steric bulk of $\mathbf{ZnL^R}$. In the case of bulky $\mathbf{ZnL^R}$ (R = *t*Bu, D*t*Bu), quenching occurs by a dynamic process that is a bimolecular electron transfer: $\mathbf{ZnL}^* + RNO_2 \rightarrow \mathbf{ZnL}^+ + RNO_2^-$. Treating this reaction with Marcus theory yielded a modest reorganization energy ($\lambda = 25$ kcal/mol), suggesting that the kinetic barriers to electron transfer from **ZnL** are similar in size to those for common biological redox cofactors.[19,20] Electronic structure calculations indicate that the dominant contributor to the reorganization energy was the outer-sphere reorganization, suggesting that a judicious choice of solvent may alter the quenching efficiency.

Experimental Section

All chemicals were purchased from Aldrich and Fisher Scientific and used as received unless specified. Solvents were purchased from VWR scientific and dried and distilled from CaH_2 (MeCN) or Mg (EtOH). Phenylenediamine was recrystallized from water and stored in an inert atmosphere glovebox (VAC Atmospheres) until use. NMR solvents were purchased from Cambridge Isotope Laboratories and used as received. Elemental analyses (C, H, and N) were performed at the University of Massachusetts mircoanalysis laboratory. Electronic structure calculations were performed with Gaussian 03, revision C.01, on a Linux computer and visualized with the GaussView 3.07 software.[21] $\mathbf{ZnL^H}$(EtOH) was geometry-optimized and the electronic structure calculated in C_1 point-group symmetry, with the spin-restricted B3LYP basis set using the Yang−Lee−Par correlation functional[22] and LanL2DZ method. The crystallographic coordinates were uploaded, and hydrogens replaced the *tert*-butyl substituents. This structure was then geometry-optimized. The electronic structure of $[\mathbf{ZnL^H}(EtOH)]^+$ was geometry-optimized and calculated at the B3LYP−LanL2DZ, spin-unrestricted level using the same initial coordinates and hydrogen replacement as for the ground-state calculation.

$\mathbf{ZnL^{DtBu}}$ ($\mathbf{H_2L^{DtBu}}$ = *N*,*N*′-Phenylene-bis(3,5-di-*tert*-butylsalicylideneimine)). To a flask of dry EtOH were added *ortho*-phenylenediamine (0.5 mmol) and 3,5-di-*tert*-butyl-salicylaldehyde (1 mmol) and refluxed overnight. The reaction mixture was filtered, and a yellow solid, $\mathbf{H_2L^{DtBu}}$ was collected. $\mathbf{H_2L^{DtBu}}$ (0.5mmol) was dissolved in EtOH with heat, and a solution of $Zn(OAc)_2$ (0.5 mmol) in EtOH was added dropwise. The solution was refluxed for 2 h and cooled to room temperature. The solid product was filtered and recrystallized. $\mathbf{ZnL^{tBu}}$ was synthesized similarly.

$\mathbf{ZnL^{OMe}}$ ($\mathbf{H_2L^{OMe}}$ = *N*,*N*′-Phenylene-bis(5-methoxy-salicylideneimine)). Dry EtOH, *ortho*-phenylenediamine (0.5 mmol), and $Zn(OAc)_2$ (0.5 mmol) were added to a flask and stirred at 80 °C

(10) Thomas, S. W.; Amara, J. P.; Bjork, R. E.; Swager, T. M. *Chem. Commun.* **2005**, (36), 4572–4574.
(11) Yang, J. S.; Swager, T. M. *J. Am. Chem. Soc.* **1998**, *120* (21), 5321–5322.
(12) Juan, Z.; Swager, T. M. *Adv. Polym. Sci.* **2005**, *177*, 151–179.
(13) Sohn, H.; Sailor, M. J.; Magde, D.; Trogler, W. C. *J. Am. Chem. Soc.* **2003**, *125* (13), 3821–3830.
(14) Sohn, H.; Calhoun, R. M.; Sailor, M. J.; Trogler, W. C. *Angew. Chem., Int. Ed.* **2001**, *40* (11), 2104–2105.
(15) Splan, K. E.; Massari, A. M.; Morris, G. A.; Sun, S. S.; Reina, E.; Nguyen, S. T.; Hupp, J. T. *Eur. J. Inorg. Chem.* **2003**, (12), 2348–2351.
(16) Cozzi, P. G.; Dolci, L. S.; Garelli, A.; Montalti, M.; Prodi, L.; Zaccheroni, N. *New J. Chem.* **2003**, *27* (4), 692–697.
(17) (a) Germain, M. E.; Vargo, T. R.; Khalifah, P. G.; Knapp, M. J. *Inorg. Chem.* **2007**, *46* (11), 4422–4429. (b) Germain, M. E.; Knapp, M. J. *J. Am. Chem. Soc.* **2008**,in press.
(18) Lanznaster, M.; Hratchian, H. P.; Heeg, M. J.; Hryhorczuk, L. M.; McGarvey, B. R.; Schlegel, H. B.; Verani, C. N. *Inorg. Chem.* **2006**, *45* (3), 955–957.
(19) Davidson, V. L.; Jones, L. H. *Biochemistry* **1996**, *35* (25), 8120–8125.
(20) Ferrari, D.; Merli, A.; Peracchi, A.; Di Valentin, M.; Carbonera, D.; Rossi, G. L. *BBA Proteins Proteom.* **2003**, *1647* (1−2), 337–342.
(21) Frisch, M. J.; Trucks, G. W.; Schlegel, H. B.; Scuseria, G. E.; Robb, M. A.; Cheeseman, J. R.; Montgomery, J. A.; Vreven, T.; Kudin, K. N.; Burant, J. C.; Millam, J. M.; Iyengar, S. S.; Tomasi, J.; Barone, V.; Mennucci, B.; Cossi, M.; Scalmani, G.; Rega, N.; Petersson, G. A.; Nakatsuji, H.; Hada, M.; Ehara, M.; Toyota, K.; Fukuda, R.; Hasegawa, J.; Ishida, M.; Nakajima, T.; Honda, Y.; Kitao, O.; Nakai, H.; Klene, M.; Li, X.; Knox, J. E.; Hratchian, H. P.; Cross, J. B.; Adamo, C.; Jaramillo, J.; Gomperts, R.; Stratmann, R. E.; Yazyev, O.; Austin, A. J.; Cammi, R.; Pomelli, C.; Ochterski, J. W.; Ayala, P. Y.; Morokuma, K.; Voth, G. A.; Salvador, P.; Dannenberg, J. J.; Zakrzewski, V. G.; Dapprich, S.; Daniels, A. D.; Strain, M. C.; Farkas, O.; Malick, D. K.; Rabuck, A. D.; Raghavachari, K.; Foresman, J. B.; Ortiz, J. V.; Cui, Q.; Baboul, A. G.; Clifford, S.; Cioslowski, J.; Stefanov, B. B.; Liu, G.; Liashenko, A.; Piskorz, P.; Komaromi, I.; Martin, R. L.; Fox, D. J.; Keith, T.; Al-Laham, M. A.; Peng, C. Y.; Nanayakkara, A.; Challacombe, M.; Gill, P. M. W.; Johnson, B.; Chen, W.; Wong, M. W.; Gonzalez, C.; Pople, J. A. *Gaussian 03*, revision C.01; Gaussian, Inc.: Wallingford, CT, 2004.
(22) Lee, C. T.; Yang, W. T.; Parr, R. G. *Phys. Rev. B: Condens. Matter Mater. Phys.* **1988**, *37* (2), 785–789.

Scheme 1. ZnL Complexes and Quenchers[a]

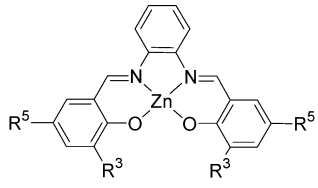

ZnL^{H} R^3=H, R^5=H
ZnL^{OMe} R^3=H, R^5=OMe
ZnL^{DtBu} R^3=tBu, R^5=tBu
ZnL^{tBu} R^3=H, R^5=tBu
ZnL^{Cl} R^3=H, R^5=Cl
ZnL^{NO2} R^3=H, R^5=NO_2

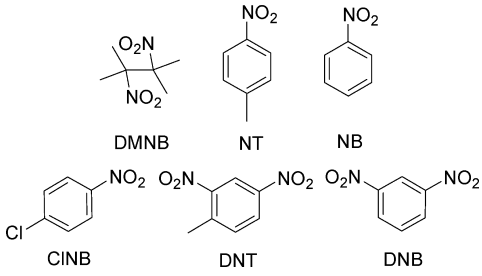

[a] DMNB = 2,3-dimethyl-2,3-dinitrobutane, NT = nitrotoluene, NB = nitrobenzene, ClNB = chloronitrobenzene, DNT = dinitrotoluene, DNB = dinitrobenzene.

for 20 min. The substituted salicylaldehyde (1 mmol) was dissolved in a minimum amount of EtOH at 80 °C, and the solution was added to the flask. The resulting solution was refluxed for 1 h and cooled. The precipitate was collected by vacuum filtration and recrystallized. A similar approach was used to prepare and purify $\mathbf{ZnL^{NO2}}$ and $\mathbf{ZnL^{Cl}}$.

$\mathbf{ZnL^{DtBu}}$. Bright orange crystals of Zn**L**(EtOH)·EtOH were collected and analyzed, as described previously.[17a]

$\mathbf{ZnL^{tBu}}$. $\mathbf{ZnL^{tBu}}$ was isolated as a yellow solid and recrystallized from EtOH (75%). ^{1}H NMR (400 MHz, DMSO 99.9%): δ 9.04 (s, 1H), 7.92 (dd, 1H, J = 3.2, 6.0 Hz), 7.35 (m, 3H), 6.66 (dd, 1H, J = 8.8 Hz).

$\mathbf{ZnL^{OMe}}$. $\mathbf{ZnL^{OMe}}$ was isolated as a red solid and recrystallized from MeOH/DMF (92%). ^{1}H NMR (400 MHz, DMSO 99.9%): δ 9.02 (s, 1H), 7.88 (dd, 1H, J = 3.6, 6.4 Hz), 7.37 (dd, 1H, J = 3.2, 6.0 Hz), 6.97 (m, 2H), 6.66 (dd, 1H, J = 9.6 Hz), 3.70 (s, 3H). Anal. calcd for $C_{22}H_{18}N_2O_4Zn\cdot H_2O$: C, 57.72; H, 4.40; N, 6.12. Found: C, 57.15; H, 4.33; N, 5.93.

$\mathbf{ZnL^{Cl}}$. $\mathbf{ZnL^{Cl}}$ was isolated as a yellow solid and recrystallized from MeOH/DMF (80%). ^{1}H NMR (400 MHz, DMSO 99.9%): δ 9.02 (s, 1H), 7.88 (dd, 1H, J = 3.2, 6.0 Hz), 7.50 (d, 1H, J = 3.2 Hz), 7.45 (dd, 1H, J = 3.6, 6.0 Hz), 7.22 (dd, 1H, J = 3.2, 9.2 Hz), 6.72 (d, 1H, J = 8.8 Hz). Anal. calcd for $C_{20}H_{12}N_2O_2Cl_2Zn\cdot H_2O$: C, 51.48; H, 3.02; N, 6.00. Found: C, 51.09; H, 3.16; N, 6.00.

$\mathbf{ZnL^{NO_2}}$. $\mathbf{ZnL^{NO_2}}$ was isolated as a yellow solid and was recrystallized from EtOAc/DMSO (80%). ^{1}H NMR (400 MHz, DMSO): δ 9.22 (s,1H), 8.61 (d, 1H J = 3.2 Hz), 8.08 (dd, 1H, J = 9.6, 2.8 Hz), 7.97 (dd, 1H, J = 3.6, 6.4 Hz), 7.49 (dd, 1H, J = 6.0, 3.2 Hz), 6.77 (d, 1H, J = 9.6 Hz). Anal. calcd for $C_{21}H_{16}N_4O_6Zn\cdot 3H_2O$: C, 45.86; H, 3.46; N, 10.70. Found: C, 45.63; H, 3.51; N, 9.24.

Optical Spectroscopy. Absorption spectra were collected on a Hewlett-Packard 8453 UV−vis spectrophotometer, and fluorescence quantum-yield measurements were performed on a JASCO FP-6500 spectrofluorimeter in dry acetonitrile. Quantum yield measurements were performed with a 1-cm-path-length quartz cuvette, using an excitation wavelength of 400 nm. The peak emission intensity of $\mathbf{ZnL^R}$ was plotted against solution absorbances to generate a linear plot to calculate the quantum yield. Quinine sulfate was used as the emission quantum-yield standard (ϕ = 0.54 in 0.1 M H_2SO_4), with an excitation wavelength of 400 nm and an emission wavelength of 460 nm. Variable-temperature steady-state fluorescence data were collected on a Photon Technology International (PTI) (TCM1000, MD5020, TC125) spectrophotometer in dry acetonitrile, using a 1 cm quartz cuvette. Quenching efficiencies (K_{SV}) were measured at the peak emission wavelength for each $\mathbf{ZnL^R}$.

Electrochemistry. Electrochemical measurements were performed in dry acetonitrile (distilled over CaH_2) on a BAS CV50W cyclic voltammeter at 100 mV/s using Fc/Fc^+ as an internal standard, 0.1 M tetrabutylammonium hexafluorophosphate (98%) as a supporting electrolyte, Pt electrodes (working and auxiliary), and Ag/Ag^+ as a pseudoreference electrode.

Magnetic Resonance Spectroscopy. ^{1}H NMR spectra were collected in d_2-methylenechloride (99.9% D), d_6-dimethylsulfoxide (99.9% D), or d_3-acetonitrile (99.8% D) with a Bruker 400 MHz (400.13 MHz) spectrometer, using the residual solvent signal as a reference. EPR spectra were collected in 3 mm quartz tubes using a Bruker ELEXSYS E-500 X-band spectrometer, with the temperature maintained at 77 K through the use of a liquid-N_2 dewar.

Emission Lifetimes. Photoluminescence decays were measured by the time-correlated single-photon counting method.[23] A frequency-doubled Nd:YVO_4 diode-pumped solid-state laser (Spectra-Physics Millennia Vs) was used to pump a mode-locked Ti:sapphire laser (KMLabs). The Ti:sapphire laser produced a train of 100 fs pulses at a repetition rate of 100 MHz and a photon wavelength of 800 nm. These pulses were frequency-doubled to 400 nm in a BBO crystal and then directed onto the sample. Fluorescence from the samples was collected and focused onto the entrance slit of a 1/8-m-focal-length spectrometer with a 4 nm spectral bandpass. The detector was a high-speed photon counting photomultiplier tube (PMH-100, Becker & Hickl, Berlin); the gating detector was a high-speed photodiode (PHD-400, Becker & Hickl), and the timing and data collection electronics were contained on a PC card (SPC-430, Becker & Hickl). The instrument response function had a width of 194 ps (fwhm), and lifetimes were determined by iterative least-squares reconvolution[24] in MathCad 7.0. In all cases, satisfactory fits were obtained by assuming that the model function obeyed a single exponential decay.

Fluorescence Microscopy. Fluorescence lifetimes were measured by time-correlated photon counting measurements.[25,26] $\mathbf{ZnL^R}$ solutions were deposited in vials fitted on clean coverslips on a Nikon Eclipse-TE2000U inverted microscope with a 1.3 NA 100× oil objective. Samples were excited with a 355 nm source from the third harmonic of a diode-pumped Nd^{3+} laser at a 76 MHz repletion rate and a pulse width of 50 ps (fwhm). An average power of 150 μW was delivered through the objective into the sample. Fluorescence was collected through the same objective through a 400 nm long-pass filter. A Perkin-Elmer Optoelectronic, SPCM-AQR-14 avalanche photodiode connected to a TimeHarp 200 time-

(23) Lewis, C.; Ware, W. R.; Doemeny, L. J.; Nemzek, T. L. *Rev. Sci. Instrum.* **1973**, *44* (2), 107–114.
(24) O'Connor, D. V.; Ware, W. R.; Andre, J. C. *J. Phys. Chem.* **1979**, *83* (10), 1333–1343.
(25) Early, K. T.; McCarthy, K. D.; Hammer, N. I.; Odoi, M. Y.; Tangirala, R.; Emrick, T.; Barnes, M. D. *Nanotechnology* **2007**, *18*, 42.
(26) Odoi, M. Y.; Hammer, N. I.; Early, K. T.; McCarthy, K. D.; Tangirala, R.; Emrick, T.; Barnes, M. D. *Nano Lett* **2007**, *7* (9), 2769–2773.

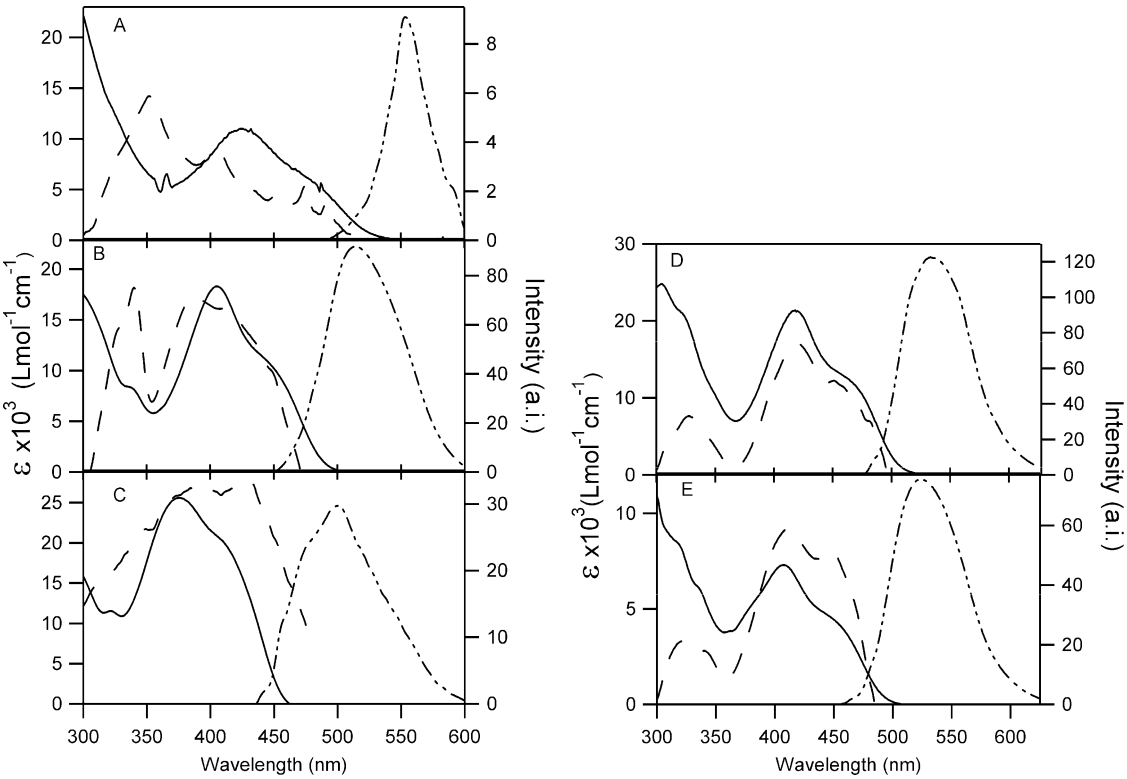

Figure 1. Absorption (solid lines), excitation (dashed lines), and emission spectra (dotted lines) of $\mathbf{ZnL^R}$ in acetonitrile. (A) $\mathbf{ZnL^{OMe}}$, (B) $\mathbf{ZnL^{Cl}}$, (C) $\mathbf{ZnL^{NO_2}}$, (D) $\mathbf{ZnL^{D/Bu}}$, (E)$\mathbf{ZnL^{tBu}}$.

to-digital converter PCI board (Picoquant GmBH) was used to record the relative arrival times of the fluorescence photons from the sample. All measurements were carried out in the time-tagged time-resolved (TTTR) mode. Fluorescence decay curves were extracted from the TTTR data for all of the samples and least-squares fitted to a single lifetime with an instrument response function of 550 ps fwhm.

Results and Discussion

ZnL*, a Highly Reducing Excited State. The **ZnL** complexes absorb light in the near-UV range ($\lambda_{max} \sim 400$ nm) and, when irradiated, emitted visible light ($\lambda_{em} \sim 530$ nm), as seen in related complexes.[15,17a] Consequently, the energy gap between the ground state and emissive excited state (E_{00}) was estimated as ~2.5 eV. Electron-donating substituents in the phenolate ring caused the absorbance and emission maxima to red-shift, from $\lambda_{max} = 376$ nm and $\lambda_{em} = 496$ nm for $\mathbf{ZnL^{NO_2}}$ to $\lambda_{max} = 430$ nm and $\lambda_{em} = 556$ nm for $\mathbf{ZnL^{OMe}}$ (Figure 1). This red shift is consistent with assigning this lowest-energy electronic transition to a $\pi-\pi^*$ transition which is largely localized on the phenolate rings, as increased electron donation would destabilize the filled π orbitals.

The fluorescence quantum yield was generally very high for **ZnL**, $\Phi \approx 0.35$, indicating that these complexes may hold promise for photochemical reactions, sensors, or OLEDs.[27,28] The $\mathbf{ZnL^{OMe}}$ complex exhibited a low quantum yield, possibly due to additional flexibility of the methoxy substituent enhancing the rates of internal conversion. The fluorescence lifetimes were measured as less than 1 ns, with the exception of the $\mathbf{ZnL^{OMe}}$ complex, which was insufficiently fluorescent for observation. This lifetime is moderate but, when paired with the high quantum yield, suggests the potential for photoinduced chemistry.

Table 1. Excited State Oxidation Potentials

	$E_{1/2}$ (V)[a], ($\mathbf{ZnL^+/ZnL}$)	ΔE_p (mV)	E_{00} (V)	$E_{1/2}$ (V),[a,b] ($\mathbf{ZnL^+/ZnL^*}$)	τ (ns)	Φ
$\mathbf{ZnL^{OMe}}$	0.23[c]	irrev.	2.41	−2.18		0.002
$\mathbf{ZnL^{D/Bu}}$	0.373	115	2.59	−2.22	0.218	0.35
$\mathbf{ZnL^{tBu}}$	0.46[c]	65	2.69	−2.23	0.217	0.27
$\mathbf{ZnL^{Cl}}$	0.687	irrev.	2.74	−2.05	0.035	0.39
$\mathbf{ZnL^{NO_2}}$	1.06	irrev.	2.84	−1.78	0.087	0.36

[a] vs $fc^{+/0}$. [b] Estimated by $E_{1/2}(\mathbf{ZnL^+/ZnL^*} = E_{1/2}(\mathbf{ZnL^+/ZnL}) - E_{00}$. [c] Taken as the oxidative peak in the CV scan.

Electron-donating substituents on the phenolate ring stabilized the one-electron oxidized ground state, $\mathbf{ZnL^+}$, as shown by cyclic voltammetry (Table 1). $E_{1/2}$ ranged from +1.05 V (vs $Fc^{+/0}$) for $\mathbf{ZnL^{NO_2}}$ to +0.23 V for $\mathbf{ZnL^{OMe}}$, values which are similar to those reported for metal phenolate/phenoxyl radical complexes.[29,30] As $\mathbf{ZnL^+}$ is a metal-coordinated phenoxyl radical, the decreasing redox potential for $\mathbf{ZnL^R}$ with stronger electron-donor substituents is attributed to a destabilization of filled π orbitals by inductive effects.

(27) Burdette, S. C.; Frederickson, C. J.; Bu, W. M.; Lippard, S. J. *J. Am. Chem. Soc.* **2003**, *125* (7), 1778–1787.
(28) de Bettencourt-Dias, A. *J. Chem. Soc., Dalton Trans.* **2007**, (22), 2229–2241.
(29) Biava, H.; Palopoli, C.; Shova, S.; De Gaudio, M.; Daier, V.; Gonzalez-Sierra, M.; Tuchagues, J. P.; Signorella, S. *J. Inorg. Biochem.* **2006**, *100* (10), 1660–1671.
(30) Itoh, S.; Kumei, H.; Nagatomo, S.; Kitagawa, T.; Fukuzumi, S. *J. Am. Chem. Soc.* **2001**, *123* (10), 2165–2175.

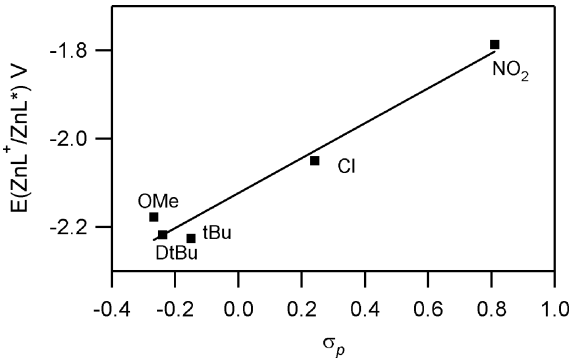

Figure 2. Correlation of the excited-state oxidation potential for $\mathbf{ZnL^R}$ (R = OMe, DtBu, tBu, Cl, NO_2) with the Hammett substituent constant.

The ground-state oxidation potentials for $\mathbf{ZnL^R}$ ranged from irreversible (R = OMe, Cl, NO_2) to quasi-reversible (R = *t*Bu, D*t*Bu), most likely due to the tendency of phenoxyl radicals to undergo subsequent chemistry. Only substituents which were bulky stabilized the $\mathbf{ZnL^+}$ radical sufficiently for observation of a reductive return wave; consequently, the thermodynamic potential for certain $\mathbf{ZnL^R}$ (R = OMe, Cl, NO_2) may be less positive than reported, by some 50 mV.

Excited-state electron transfers will be governed by the excited-state oxidation potential, as this represents the thermodynamic drive for the excited state to donate an electron to form the phenoxyl radical $\mathbf{ZnL^+}$. The excited-state oxidation potentials, $E(\mathbf{ZnL^+/ZnL^*})$, were obtained as the difference between the measured ground-state oxidation potential ($E_{1/2}$) and the energy gap between the ground and excited states (E_{00}). E_{00} was estimated as the frequency at which the emission band exhibited 1% of it is maximum intensity,[31,32] with E_{00} ranging from 2.41 to 2.84 eV. These values were then used to calculate $E(\mathbf{ZnL^+/ZnL^*})$ as 1.79−2.23 V, indicating that **ZnL*** is a very powerful electron donor.

A linear free energy correlation between $E(\mathbf{ZnL^+/ZnL^*})$ and the Hammett substituent constants for the substituted phenolate rings, σ_p, exhibited a positive slope (Figure 2).[33] The excited-state becomes more reducing with electron-donating substituents, as shown by a more negative oxidation potential. Similar effects have been observed for enzymatic systems and metal−phenolate complexes where electron-donating groups are well-known to stabilize phenoxyl radicals.[34–36]

Scheme 2. Static and Collisional Quenching Pathways for **ZnL***

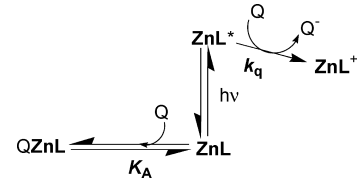

Mixed Quenching Pathways for ZnL. The highly reducing properties of **ZnL*** clearly indicated that fluorescence quenching by nitro-alkanes or nitro-aromatics could occur by electron transfer.[17a] However, further consideration of the highest occupied molecular orbital/lowest unoccupied molecular orbital (HOMO/LUMO) gaps, and spectral overlaps, for representative compounds excluded the possibility of simple energy transfer as a quenching mechanism. First, the emission bands of $\mathbf{ZnL^R}$ (Figure 1) are well-separated from the absorption bands found for typical nitroaromatics ($\lambda_{abs} \sim 400$ nm), indicating that quenching by resonance energy transfer cannot occur. Second, the excited state of $\mathbf{ZnL^R}$ ($E_{00} < 2.9$ eV) is much lower in energy than the excited state of the typical nitroaromatic nitrobenzene ($E_{00} \sim 4.5$ eV, on the basis of the low-energy side of the absorption band), indicating that collisional energy transfer cannot happen.[17a,32]

While electron transfer is the most reasonable mechanism to propose on the basis of thermodynamic considerations, two distinct pathways could lead to quenching.[37] Static quenching of fluorescence is a ground-state process in which the quencher binds to the ground-state of **ZnL**, forming a nonfluorescent Q**ZnL** adduct with the association constant K_A. Dynamic quenching is an excited-state process, in that the quencher collides with the excited state **ZnL***, thereby deactivating the excited state with a bimolecular rate constant of k_q. Steady-state and transient fluorescence quenching experiments were performed to discriminate between the static and dynamic pathways, on the basis of a minimal mechanism (Scheme 2).

This mechanistic scheme leads to the Stern-Volmer equation (eq 1), in which the normalized fluorescence intensity (I_0/I) is a function of static (K_A) and dynamic quenching ($k_q\tau_0$) terms.

$$I/I_0 = (1 + K_A[Q])(1 + k_q\tau_0[Q]) \quad (1)$$

In the limiting cases in which one term dominates quenching (i.e., $K_A \ll k_q\tau_0$ or $K_A \gg k_q\tau_0$), I_0/I will be a linear function of $[Q]$, in which the slope is the observed quenching efficiency (K_{SV}). The quenching efficiency can therefore represent either K_A for static quenching or $k_q\tau_0$ for dynamic quenching.

Steady-state fluorescence quenching experiments were carried out, in which the fluorescence intensity of **ZnL** (20 μM in CH_3CN) decreased in a dose-dependent manner upon the addition of aliquots from a stock solution of DNT (400 mM, CH_3CN). Three $\mathbf{ZnL^R}$ (R = *t*Bu, D*t*Bu, Cl) complexes exhibited linear Stern-Volmer quenching responses to DNT (Figure 3A), which may reflect the steric bulk of those

(31) Petersen, J. D.; Watts, R. J.; Ford, P. C. *J. Am. Chem. Soc.* **1976**, *98* (11), 3188–3194.
(32) Dossing, A.; Ryu, C. K.; Kudo, S.; Ford, P. C. *J. Am. Chem. Soc.* **1993**, *115* (12), 5132–5137.
(33) Ford, R. A. G.; Arnold J. *The Chemist's Companion A*; Wiley-Interscience Publication: New York, 1972.
(34) Badeau, M.; Adlercreutz, H.; Kaihovaara, P.; Tikkanen, M. J. *J. Steroid. Biochem.* **2005**, *96* (3−4), 271–278.
(35) Burton, G. W.; Doba, T.; Gabe, E. J.; Hughes, L.; Lee, F. L.; Prasad, L.; Ingold, K. U. *J. Am. Chem. Soc.* **1985**, *107* (24), 7053–7065.
(36) Itoh, S.; Takayama, S.; Arakawa, R.; Furuta, A.; Komatsu, M.; Ishida, A.; Takamuku, S.; Fukuzumi, S. *Inorg. Chem.* **1997**, *36* (7), 1407–1416.
(37) Lakowicz, J. R. *Principles of Fluorescence Spectroscopy*; Plenum Press: New York, 1986.
(38) Swadesh, J. K.; Mui, P. W.; Scheraga, H. A. *Biochemistry* **1987**, *26* (18), 5761–5769.
(39) Vaughan, W. M.; Weber, G. *Biochemistry* **1970**, *9* (3), 464–473.
(40) Lehrer, S. S. *Biochemistry* **1971**, *10* (17), 3254–3263.

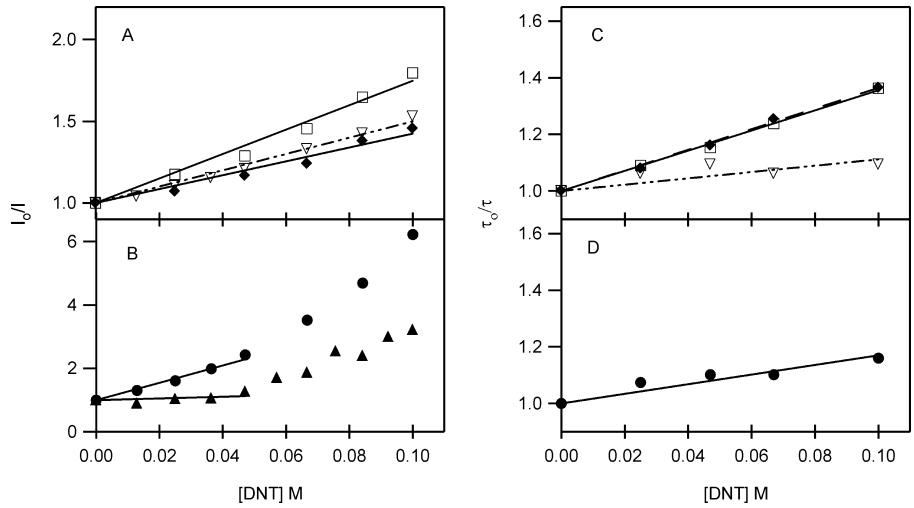

Figure 3. Stern-Volmer plots for the quenching of $\mathbf{ZnL^R}$ (20 μM, CH_3CN) by DNT. Steady state data: (A) $\mathbf{ZnL^{DtBu}}$ (open squares), $\mathbf{ZnL^{tBu}}$ (diamonds), $\mathbf{ZnL^{Cl}}$ (inverted triangles); (B) $\mathbf{ZnL^{NO_2}}$ (circles) and $\mathbf{ZnL^{OMe}}$ (triangles). Time-resolved data: (C) $\mathbf{ZnL^{DtBu}}$ (open squares), $\mathbf{ZnL^{tBu}}$ (diamonds), $\mathbf{ZnL^{Cl}}$ (inverted triangles); (D) $\mathbf{ZnL^{NO_2}}$ (circles).

substituents. The quenching efficiencies were modest, with K_{SV} (M^{-1}) = 7.5 ± 0.3, 4.2 ± 0.2, and 4.9 ± 0.1 for $\mathbf{ZnL^{DtBu}}$, $\mathbf{ZnL^{tBu}}$, and $\mathbf{ZnL^{Cl}}$, respectively. The time-resolved Stern-Volmer quenching of these complexes with DNT (Figure 3C) was also linear, but with reduced quenching efficiencies: K_{SV} (M^{-1}) = 3.6 ± 0.1, 3.6 ± 0.1, and 1.7 ± 0.2, respectively. This indicated that $\mathbf{ZnL^{DtBu}}$, $\mathbf{ZnL^{tBu}}$, and $\mathbf{ZnL^{Cl}}$ were quenched by the dynamic pathway and suggested that the discrepancy between the steady-state and time-resolved quenching efficiencies were due to the absorption of incident radiation (λ_{ex} = 400 nm) at high concentrations of DNT.

Two $\mathbf{ZnL^R}$ (R = OMe, NO_2) complexes exhibited curved steady-state quenching curves (Figure 3B), indicating that both static and dynamic pathways were significant for quenching. The ground-state binding constant was estimated by fitting the quenching data in the limit of low [DNT] to eq 1 with K_A = 2.62 ± 0.03 M^{-1} ($\mathbf{ZnL^{OMe}}$) and 27.26 ± 0.06 M^{-1} ($\mathbf{ZnL^{NO_2}}$). These association constants are consistent with the weak binding of small ligand binding to $\mathbf{ZnL^{DtBu}}$ in CH_2Cl_2 solution.[17a] The time-resolved Stern-Volmer quenching efficiency for $\mathbf{ZnL^{NO_2}}$ was very small, K_{SV} = 1.1 ± 0.2 M^{-1} (Figure 3D), indicating that the static pathway was dominant in this case; we were unable to measure the fluorescence lifetime of $\mathbf{ZnL^{OMe}}$. While the dynamic pathway was more important for $\mathbf{ZnL^R}$ with the bulkiest subsitutents (R = *t*Bu, D*t*Bu), the presence of multiple quenching pathways offers an explanation for the success of a $\mathbf{ZnL^R}$-based sensor array to discriminate nitroaromatics.[17b]

Diffusional Analysis of Mixed Quenching Pathways. To further differentiate between the static and dynamic quenching pathways, a variable-temperature fluorescence quenching experiment was performed with those complexes exhibiting linear Stern-Volmer quenching: $\mathbf{Zn^{DtBu}}$, $\mathbf{Zn^{tBu}}$, and $\mathbf{Zn^{Cl}}$. As the rate of bimolecular collision is proportional to temperature, but inversely proportional to viscosity (η), the quenching efficiency (K_{SV}) for a dynamic quenching pathway should exhibit a similar dependence, $(K_{SV}/I_0) \propto (T/\eta)$, in which K_{SV} has been normalized to the fluorescence intensity in the absence of a quencher (I_0).[38–43] Steady-state quenching efficiency using DNT was measured at 0, 15, and 25 °C with $\mathbf{ZnL^{DtBu}}$, $\mathbf{ZnL^{tBu}}$, and $\mathbf{ZnL^{Cl}}$ (20 μM). The predicted linear dependence was observed, indicating that quenching in these cases predominantly follows the dynamic pathway (Figure 4). However, the quenching efficiencies for $\mathbf{ZnL^{DtBu}}$ and $\mathbf{ZnL^{tBu}}$ extrapolated to near-zero as T/η approaches zero, as expected for a dominant dynamic quenching pathway; however, the intercept for $\mathbf{ZnL^{Cl}}$ was nonzero, which suggested that a static pathway also contributed to quenching in this case.

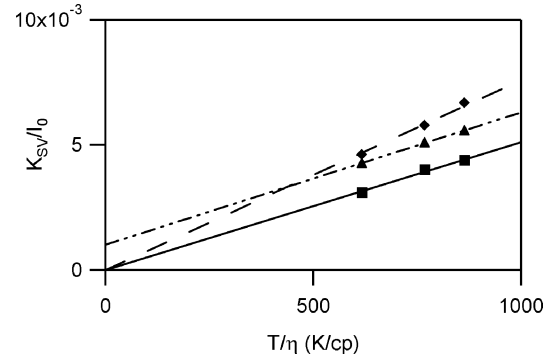

Figure 4. Viscosity dependence of steady-state quenching efficiency of DNT with $\mathbf{ZnL^{tBu}}$ (diamonds), $\mathbf{ZnL^{DtBu}}$ (squares), and $\mathbf{ZnL^{Cl}}$(triangles).

Aggregation at Elevated ZnL Concentration. In view of the mixed quenching pathway for those $\mathbf{ZnL^R}$'s with less bulky substituents, the fluorescence lifetime and quenching were investigated under conditions which encouraged molecular aggregation. The quenching of $\mathbf{ZnL^R}$ at high fluoropohore concentrations was monitored by transient methods using a fluorescence microscope, to minimize the optical path length. Transient quenching experiments were performed at a 2.6 mM $\mathbf{ZnL^R}$ concentration and varied concentrations of nitrobenzene as the quencher (Table 2).

(41) Bordbar, M.; Shamsipur, M.; Alizadeh, N. *J. Photochem. Photobiol., A* **2006**, *178* (1), 83–89.
(42) Birks, J. B.; Najjar, H. Y.; Lumb, M. D. *J. Phys. B* **1971**, *4* (11), 1516–1522.
(43) Moon, A. Y.; Poland, D. C.; Scheraga, H. A. *J. Phys. Chem.* **1965**, *69* (9), 2960–2966.

Table 2. Fluorescence Lifetimes and Transient Quenching with Nitrobenzene at High [**ZnL**][a]

	τ_0 (ns)	K_{SV} (M^{-1})
ZnL^{OMe}		
ZnL^{DtBu}	0.9	0.3 ± 0.2
ZnL^{tBu}	0.7	1.8 ± 0.4
ZnL^{Cl}	1.2	1.5 ± 0.6
ZnL^{NO2}	1.3	1.4 ± 0.8

[a] [**ZnL^{R}**] = 2.6 mM.

The fluorescence data for **ZnL^{R}** under high-concentration conditions were suggestive of molecular excimer formation. The fluorescence lifetimes for concentrated **ZnL^{R}** were longer than under optically dilute conditions and were nearly unaffected by the addition of a quencher. Pyrene, for example, is known to form dimers with longer fluorescence lifetimes than found for the monomer. The near-zero values for K_{SV} clearly indicated that the dynamic quenching pathway was less important under concentrated **ZnL^{R}** conditions, but this could reflect underlying optical artifacts. While we were unable to further characterize the **ZnL^{R}**—NB interactions under these conditions due to the low fluorescence intensity, we note that even the sterically bulky **ZnL^{R}**'s appear to aggregate in solution.

Formation of a Phenoxyl Radical upon Photolysis. The quenching of **ZnL*** was proposed to follow an electron-transfer mechanism, on the basis of the correlation between quenching efficiency and excited-state oxidation potential[17a] and thermodynamic analysis described above. As an electron-transfer quenching mechanism predicts that photolysis of **ZnL** in the presence of DNB would form the{**ZnL**$^{+}$ DNB^{-}} radical pair, photolysis was performed on **ZnL** mixed with DNB within an X-band EPR cavity at 77K.

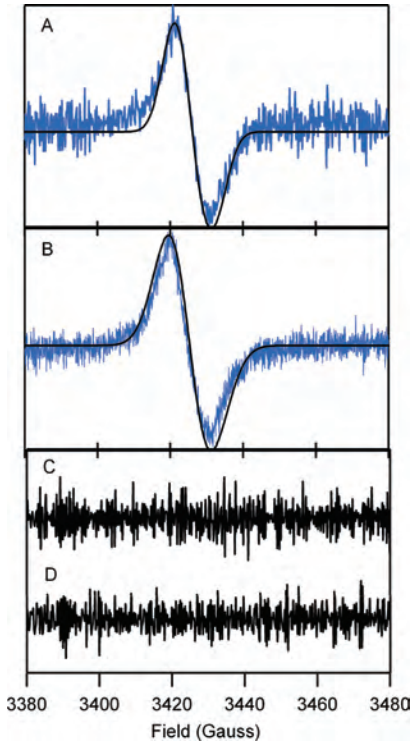

Figure 5. EPR spectra of frozen acetonitrile solutions following irradiation for 5 min (9.609 GHz). (A) **ZnL^{DtBu}** + DNB. (B) **ZnL^{tBu}** + DNB. (C) **ZnL^{DtBu}**. (D) DNB. Simulations shown as narrow solid lines.

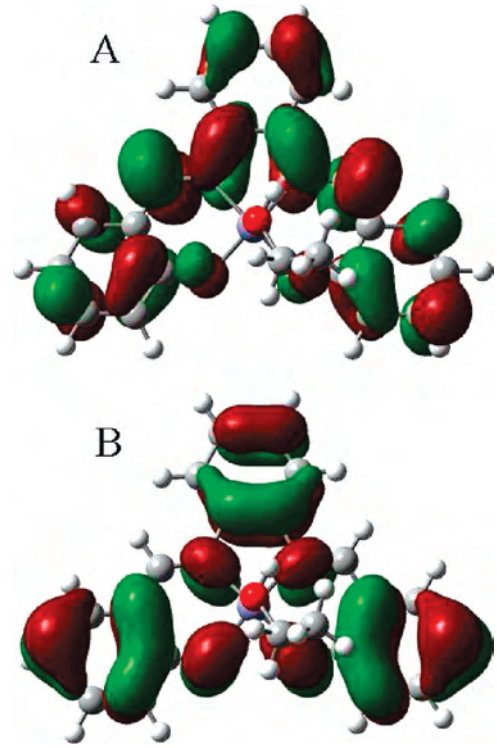

Figure 6. Orbital density surfaces of **ZnL^{H}**(EtOH) orbitals. (A) LUMO (−1.979 eV) and (B) HOMO (−5.086 eV).

Solutions of **ZnL^{DtBu}** or **ZnL^{tBu}** (1 mM, CH_3CN) were mixed with DNB (120 mM), then frozen within EPR tubes using liquid nitrogen and inserted into an X-band EPR cavity held at 77 K. A pyrex-filtered Xe lamp (passes light of $\lambda >$ 300 nm) was used to illuminate the frozen solutions for several minutes; then, EPR spectra were collected after turning the lamp off (Figure 5). Control samples of either **ZnL^{DtBu}** or DNB alone remained EPR-silent following photolysis, consistent with the absence of any radical formation. However, when both **ZnL^{DtBu}** and DNB were mixed together, frozen at 77 K, then irradiated with visible light for 5 min, the resulting solution produced an isotopic signal at $g_{eff} = 2.004$, indicating the formation of $S = 1/2$ radicals. Upon thawing and refreezing to 77 K, the radical signal disappeared, indicating that diffusion had allowed the radicals to recombine. Similarly, photolysis of a mixture of **ZnL^{tBu}** and DNB resulted in an isotropic EPR signal at $g_{eff} = 2.004$. The peak-to-trough linewidths for **ZnL^{DtBu}** and **ZnL^{tBu}** are 9.4 G and 11.3 G respectively, due to unresolved fine-structure.

These spectra were simulated using XSophe using the spin Hamiltonian $\hat{H} = \beta B_0 g \hat{S}_Z$, appropriate for anisotropic **g** tensors.[44,45] Satisfactory simulations for **ZnL^{DtBu}** were achieved by use of an anisotropic $g_x = 2.007$, $g_y = 2.004$, and $g_z = 2.000$ and an intrinsic line width of 4 G. Simulations for **ZnL^{tBu}** used similar values, with $g_x = 2.006$, $g_y = 2.004$, and $g_z = 2.000$ and intrinsic line width of 6 G. These **g** tensors are very similar to those reported for other metal-

(44) *XSophe 1.1.4*; Bruker: Madison, WI, 2004.
(45) Abragam, A.; Bleaney, B. *Electron paramagnetic resonance of transition ions*; Clarendon Press: Oxford, 1970; p xiv; p 911.

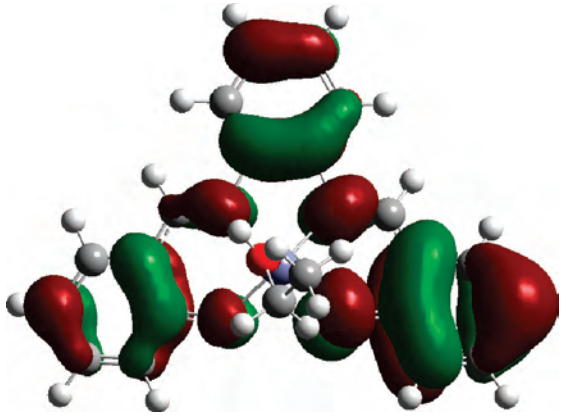

Figure 7. DFT surface of the phenoxyl radical $\mathbf{ZnL^H}(EtOH)^+$ SOMO at the B3LYP-LanL2DZ level.

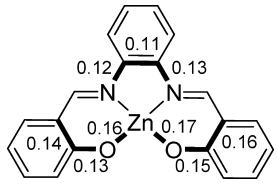

Figure 8. Bond length changes measured by DFT calculations of optimized ground-state and phenoxyl radical structures. Major structural changes indicated by bold bonds and values (Å).

coordinated phenoxyls, as expected for the $\mathbf{ZnL}^+$ radical.[46,47] The linewidths reflect a combination of unresolved superhyperfine from the protons on **ZnL** and exchange coupling within the radical pair. As the two experiments were performed under the same experimental conditions, exchange coupling should be comparable in both cases, leaving unresolved superhypefine coupling as the likely origin of the different linewidths. $\mathbf{ZnL^{tBu}}$ has one additional phenolic proton as compared to $\mathbf{ZnL^{DtBu}}$, making it likely that the former would exhibit additional superhyperfine interactions.

While the observed EPR signals are clear evidence for the formation of $\mathbf{ZnL}^+$ via a photoinduced electron transfer, these data do not resolve whether this charge transfer follows from a static or dynamic pathway (Scheme 2). If the charge transfer occurred by a dynamic quenching pathway, then the EPR signals could be attributed to that small population of **ZnL** and DNB which was frozen in close proximity, and which could transfer electrons over such relatively short distances (ca. 10 Å). In this view, back-electron-transfer would be impeded by the inability of the lattice to rearrange, which would increase the kinetic barrier to such a reaction. Conversely, the EPR signals could arise from a weak ground-state DNB−**ZnL** adduct; but we anticipate that such an adduct would undergo back-electron-transfer rapidly. Nevertheless, the transient quenching data (Figure 3) clearly show that $\mathbf{ZnL^R}$ (R = *t*Bu, D*t*Bu, Cl) are quenched by a dynamic pathway. The EPR data, and thermodynamic considerations described above, simply support the model that this quenching is due to electron transfer, and not to energy transfer.

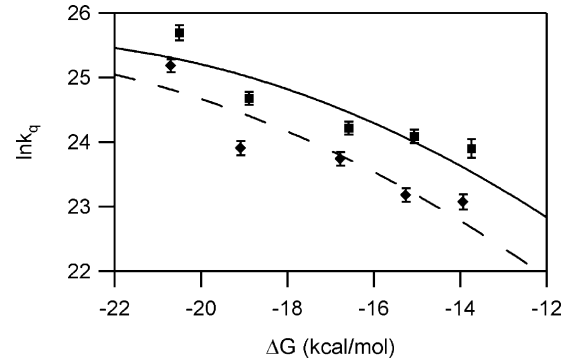

Figure 9. Driving force dependence of electron transfer between **ZnL*** and $ArNO_2$, $\mathbf{ZnL^{DtBu}}$ (triangles), and $\mathbf{ZnL^{tBu}}$ (diamonds). See the text for fitting parameters.

Electronic Structure Calculation. DFT calculations were used to better understand the physical properties of **ZnL** and $\mathbf{ZnL}^+$. The ground-state electronic structure of $\mathbf{ZnL^H}(EtOH)$ revealed a delocalized HOMO and LUMO with substantial ligand π composition. The orbital contributions were large for both the phenolate rings (62%) and the diamine ring (5%) to the HOMO. The LUMO was more localized, with a reduced contribution from the phenolate rings (40%) and an increased orbital density residing in the phenylenediamine ring (24%). Orbital density maps (Figure 6) show large contributions from the 3 and 5 positions of the phenolate rings (C-1 is the imine position), indicating that electron-donating substituents at the 5-position are well-positioned to destabilize the HOMO. This would lower the thermodynamic barrier to removing an electron to form either the excited state **ZnL*** or the one-electron oxidized state, $\mathbf{ZnL}^+$, as seen in the experimentally determined redox potentials.

The electronic structure of $[\mathbf{ZnL^H}(EtOH)]^+$ revealed a semioccupied molecular orbital (SOMO) that closely resembled a phenoxyl radical. A large percentage (53%) of the orbital contribution in the SOMO is derived from the phenoxyl moiety, while a much smaller contribution of the SOMO lies on the phenylenediamine ring (14%) (Figure 7). This is entirely consistent, viewing $\mathbf{ZnL}^+$ as a phenoxyl radical to a first approximation, as was done in explaining the EPR line shape.

In view of the electron-transfer mechanism for dynamic quenching, the computational data were also analyzed for bonding changes coincident with the $\mathbf{ZnL} \rightarrow \mathbf{ZnL}^+ + e^-$ redox conversion. Marcus theory relates the kinetic barrier to a reaction to bonding changes within the reactants, which is the inner-sphere reorganization energy (λ_i). Bonding changes were calculated from energy-minimized **ZnL** and $\mathbf{ZnL}^+$ geometries, considering only those bonds which changed bond length (Δx_n) by greater than 0.01 Å (Figure 8).[48] Assuming a harmonic oscillator with a force constant (k_n) for each bond, the inner-sphere reorganization energy for **ZnL** was calculated as $\lambda_i = 1$ kcal/mol using the equation $\lambda_i = \sum 1/2 k_n(\Delta x_n)^2$.[49] This likely reflects the large number of bonding centers which are involved in the redox process.

(46) Yamaji, T.; Saiful, I. S. M.; Baba, M.; Yamauchi, S.; Yamauchi, J. *J. Phys. Chem. A* **2007**, *111* (21), 4612–4619.
(47) Modarelli, D. A.; Lahti, P. M.; George, C. *J. Am. Chem. Soc.* **1991**, *113* (16), 6329–6330.
(48) Silverstein, R. M. W.; Francis, X. *Spectrometric Identification of Organic Compounds*, 6th ed.; John Wiley & Sons Inc.: New York, 1988.
(49) Marcus, R. A.; Sutin, N. *Biochim. Biophys. Acta* **1985**, *811* (3), 265–322.

Reorganization Energy for ZnL/ZnL$^+$ is Moderately Small. As bimolecular electron transfer with nitro-organics is the mechanism of quenching for both **ZnL$^{D\textit{t}Bu}$** and **ZnL$^{\textit{t}Bu}$** under typical conditions (Scheme 2), we turned to Marcus theory to gain insight into the rate of this reaction. Marcus theory provides a unified framework for understanding electron transfers throughout chemistry, as it relates measurable thermodynamic properties to rate constants.[49] At the simplest level, the kinetic barrier to electron transfer ($\Delta G^{\ddagger}$) is determined by the driving force (ΔG^0), which comes from relative redox potentials, and the reorganization energy (λ), which arises from bonding and solvation differences which accompany the electron transfer (Figure 9). Marcus theory predicts that the natural logarithm of the electron transfer rate (k_q') will exhibit a parabolic dependence on driving force, with a maximal rate (equal to the collisional frequency, Z) found at the point where $-\Delta G^0 = \lambda$ (eq 2).

$$\ln k_q' = \ln Z - \frac{(\lambda + \Delta G^0)^2}{(4\lambda RT)} \quad \Delta G^{\ddagger} = \frac{(\lambda + \Delta G^0)^2}{4\lambda} \qquad (2)$$

The quenching of **ZnL$^{\textit{t}Bu}$** and **ZnL$^{D\textit{t}Bu}$** (20 μM, CH_3CN) by substituted nitroaromatics was monitored by steady-state methods and fit to eq 1 to obtain the observed quenching rates (k_q). These were then corrected for diffusion, for analysis of the diffusion-corrected quenching rates (k_q'). The diffusion-corrected quenching rates were then fit to eq 2 with Z fixed at 1×10^{11} M^{-1} s^{-1}, to yield $\lambda = 24.7 \pm 0.9$ kcal/mol for **ZnL$^{D\textit{t}Bu}$** and $\lambda = 25.7 \pm 0.7$ kcal/mol for **ZnL$^{\textit{t}Bu}$**.

One very useful view of reorganization energy is as a conserved property arising from each reactant, as is done with the Marcus cross-relation. This postulates that the reorganization energy for the nitroaromatic quenching of **ZnL*** (eq 3c) is the mean of the self-exchange reorganization energies for the two redox partners (eqs 3a, 3b), $\lambda_{ZnQ} = 1/2(\lambda_{ZnZn} + \lambda_{QQ})$.[49] This allows for the intrinsic barrier to electron-transfer for a given redox partner to be benchmarked and used to predict kinetics, much as is done with half-cell potentials in predicting the thermodynamics of redox reactions.

$$\mathbf{ZnL^*} + \mathbf{ZnL^+} \rightarrow \mathbf{ZnL^+} + \mathbf{ZnL^*} \qquad (3a)$$

$$ArNO_2 + ArNO_2 \rightarrow ArNO_2^- + ArNO_2 \qquad (3b)$$

$$\mathbf{ZnL^*} + ArNO_2 \rightarrow \mathbf{ZnL^+} + ArNO_2^- \qquad (3c)$$

Taking the reorganization energy for the cross-reaction as $\lambda_{ZnQ} = 25$ kcal/mol, and $\lambda_{QQ} = 30$ kcal/mol,[50] the calculated self-exchange reorganization energy for **ZnL*/ZnL$^+$** was $\lambda_{ZnZn} = 20$ kcal/mol. This self-exchange reorganization energy is comparable to those reported for many biological redox cofactors, such as low-spin hemes found in cytochromes, blue copper sites, and the special pair in the bacterial photosystem.[19,20,49,51–53] Consequently, metal−phenolates may be robust biological redox cofactors, as suggested by the redox-active phenoxyl radicals in galactose oxidase and ribonucleotide reductase.[54,55]

The reorganization energy for the cross-reaction (eq 3c) can also be partitioned as a sum of inner-sphere (λ_i) and outer-sphere (λ_o) contributions: $\lambda = \lambda_i + \lambda_o$. The outer-sphere reorganization energy arises from changes in solvation, which reflect the sizes of **ZnL** (r_{Zn}) and Ar−NO_2 (r_Q),[56] and the optical (D_{op}) and static (D_s) dielectric constants of the acetonitrile.[57] Assuming spherical reactants, the outer-sphere reorganization energy was calculated as $\lambda_o = 19$ kcal/mol using eq 4,[49] in which ϵ_o is the permittivity of free space and e is the elementary charge.

$$\lambda_o = \frac{1}{4\pi\varepsilon_0} e^2 \left(\frac{1}{2r_{Zn}} + \frac{1}{2r_Q} - \frac{1}{r_{Zn} + r_Q}\right)\left(\frac{1}{D_{op}} + \frac{1}{D_s}\right) \qquad (4)$$

Calculations of λ_{ZnQ} from both λ_i and λ_o contributors resulted in $\lambda_{ZnQ} = 20$ kcal/mol, keeping in mind that λ_i only measures the contribution from the **ZnL*** partner. This value was in close-enough agreement with the experimental value, to show that outer-sphere reorganization was the dominant barrier to electron transfer. This suggests that altering the dielectric environment may be one way to modulate charge transfers from **ZnL**, or other metal phenolates.

Conclusions

The fluorescence of Zn(salophen) (**ZnL**) complexes is quenched by photoinduced electron transfer with nitroaromatics. The pathway for fluorescence quenching was dependent on both the excited-state oxidation potential and the bulk of the salophen ligand, with the dynamic quenching pathway dominant for bulky ligands. The Marcus cross-relation indicated a small intrinsic barrier for **ZnL***/**ZnL$^+$**, suggesting that **ZnL** may be useful for photoinduced charge transfers. Understanding the energy barriers for quenching by electron-transfer will aid in the further development of photoinduced charge transfer reactions involving Zn(salen)-type compounds.

Acknowledgment. The authors thank Prof. Paul M. Lahti for help with the EPR photolysis experiment, Robert Herbst for helpful comments, Prof. S. Thayumanavan for the use of the steady-state fluorimeter, and Prof. M. D. Barnes for access to the fluorescence microscope; the William E. McEwen Fellowship (MG); and the National Science Foundation for financial support of the EPR facility (CHE-0443180 NSF-CRIF).

Supporting Information Available: Tables of parameters for calculating λ_i, coordinates for geometry-optimized **ZnL**(EtOH) and **ZnL$^+$**(EtOH), and diffusion-corrected quenching rate constants. This material is available free of charge via the Internet at http://pubs.acs.org.

IC702469Q

(50) Ferry, J. L.; Glaze, W. H. *J. Phys. Chem. B* **1998**, *102* (12), 2239–2244.
(51) Regan, J. J.; Ramirez, B. E.; Winkler, J. R.; Gray, H. B.; Malmstrom, B. G. *J. Bioenerg. Biomembr.* **1998**, *30* (1), 35–39.
(52) DiBilio, A. J.; Hill, M. G.; Bonander, N.; Karlsson, B. G.; Villahermosa, R. M.; Malmstrom, B. G.; Winkler, J. R.; Gray, H. B. *J. Am. Chem. Soc.* **1997**, *119* (41), 9921–9922.
(53) Gray, H. B.; Malmstrom, B. G.; Williams, R. J. P. *J. Biol. Inorg. Chem.* **2000**, *5* (5), 551–559.
(54) Stubbe, J.; Nocera, D. G.; Yee, C. S.; Chang, M. C. Y. *Chem. Rev.* **2003**, *103* (6), 2167–2201.
(55) Rogers, M. S.; Dooley, D. M. *Curr. Opin. Chem. Biol.* **2003**, *7* (2), 189–196.
(56) Geometry minimized using PC Spartan 04. Quenchers assumed as 3-D spheres; r_Q estimated by averaging distances from x, y, z cartesian axes. Calculated r_Q ($\times 10^{-10}$ m): NT(3.46), NB (3.25), ClNB (3.49), DNT (4.21), DNB (3.70); r_{Zn} ($\times 10^{-10}$ m): (6.63).
(57) Kitamura, N.; Kim, H. B.; Okano, S.; Tazuke, S. *J. Phys. Chem.* **1989**, *93* (15), 5750–5756.